New Phytologist

Research

Does plant ecosystem thermoregulation occur? An extratropical assessment at different spatial and temporal scales

Zhengfei Guo[1], Christopher J. Still[2], Calvin K. F. Lee[1], Youngryel Ryu[3], Benjamin Blonder[4], Jing Wang[1], Timothy C. Bonebrake[1,5], Alice Hughes[1,5], Yan Li[6], Henry C. H. Yeung[1], Kun Zhang[1,7], Ying Ki Law[1], Ziyu Lin[1] and Jin Wu[1,5,8]

[1]School for Biological Sciences, The University of Hong Kong, Pokfulam Road, Hong Kong, China; [2]Forest Ecosystems and Society, Oregon State University, Corvallis, OR 97331, USA; [3]Department of Landscape Architecture and Rural Systems Engineering, College of Agriculture and Life Sciences, Seoul National University, Gwanak-gu, Seoul, South Korea; [4]Department of Environmental Science, Policy, and Management, University of California, Berkeley, CA 94720, USA; [5]Institute for Climate and Carbon Neutrality, The University of Hong Kong, Hong Kong, China; [6]State Key Laboratory of Earth Surface Processes and Resources Ecology, Beijing Normal University, Beijing 100875, China; [7]Department of Mathematics, The University of Hong Kong, Hong Kong, China; [8]State Key Laboratory of Agrobiotechnology, The Chinese University of Hong Kong, Shatin, Hong Kong, China

Author for correspondence:
Jin Wu
Email: jinwu@hku.hk

Received: *9 August 2022*
Accepted: *11 November 2022*

New Phytologist (2022)
doi: 10.1111/nph.18632

Key words: biotic and abiotic drivers, climate change, ecosystem thermoregulation, FLUXNET2015, limited homeothermy, megathermy, satellite.

Summary

- To what degree plant ecosystems thermoregulate their canopy temperature (T_c) is critical to assess ecosystems' metabolisms and resilience with climate change, but remains controversial, with opinions from no to moderate thermoregulation capability.
- With global datasets of T_c, air temperature (T_a), and other environmental and biotic variables from FLUXNET and satellites, we tested the 'limited homeothermy' hypothesis (indicated by T_c & T_a regression slope < 1 or $T_c < T_a$ around midday) across global extratropics, including temporal and spatial dimensions.
- Across daily to weekly and monthly timescales, over 80% of sites/ecosystems have slopes ≥1 or $T_c > T_a$ around midday, rejecting the above hypothesis. For those sites unsupporting the hypothesis, their T_c–T_a difference (ΔT) exhibits considerable seasonality that shows negative, partial correlations with leaf area index, implying a certain degree of thermoregulation capability. Spatially, site-mean ΔT exhibits larger variations than the slope indicator, suggesting ΔT is a more sensitive indicator for detecting thermoregulatory differences across biomes. Furthermore, this large spatial-wide ΔT variation (0–6°C) is primarily explained by environmental variables (38%) and secondarily by biotic factors (15%).
- These results demonstrate diverse thermoregulation patterns across global extratropics, with most ecosystems negating the 'limited homeothermy' hypothesis, but their thermoregulation still occurs, implying that slope < 1 or $T_c < T_a$ are not necessary conditions for plant thermoregulation.

Introduction

Whether plant ecosystems can thermoregulate their canopy temperature (T_c) in response to the changing environment remains a central question in plant ecology and ecophysiology (Doughty & Goulden, 2008; Pau *et al.*, 2018; Lin *et al.*, 2020; Choury *et al.*, 2022), with increasing relevance due to global climate change. T_c is a key state variable tightly regulating canopy metabolism of photosynthesis, respiration, and transpiration (Farquhar *et al.*, 1980; Bernacchi *et al.*, 2013; Lombardozzi *et al.*, 2015), which further impacts the growth and health of individual plants, as well as regional to global-scale carbon and water cycles (Lloyd & Farquhar, 2008; Dong *et al.*, 2017; Still *et al.*, 2021). Furthermore, because of the hump-shaped relationship between gross primary productivity (GPP) and T_c (e.g. Collier *et al.*, 2017; Slot & Winter, 2017), as well as the exponential relationship between T_c and plant respiration, changes in T_c in concert with global warming will strongly affect net terrestrial carbon uptake. The metabolic and hydrologic impacts of climate warming are thus strongly related to plant canopy thermoregulation, which determines the directional change and magnitude of T_c deviations from optimal temperatures for GPP (Michaletz *et al.*, 2016; Blonder & Michaletz, 2018; Huang *et al.*, 2019).

Plant thermoregulation refers to the maintenance of relatively stable T_c in the face of variable air temperature (T_a). It could result from a wide suite of structural (regulating radiation absorption and convection), morphological (regulating boundary conductance), and physiological (e.g. stomatal behavior and regulating transpiration) traits, and can be quantified in two ways: the regression slope of T_c vs T_a as well as the difference between T_c and T_a (ΔT) (Box 1). Specifically, it has been hypothesized that if thermoregulation occurs, (1) T_c will change more slowly than T_a over time,

Box 1 Definitions of different thermoregulation patterns.

Both canopy temperature (T_c) and air temperature (T_a) vary with time. The slope of T_c vs T_a (slope $= \partial T_c/\partial T_a$) describes their relative rates of change. The difference between T_c vs T_a ($\Delta T = T_c - T_a$) describes their relative magnitudes.

- Poikilothermy occurs when T_c has almost the same rate of change as T_a (slope $\approx$ 1; a conservative range of 0.9–1.1 was used; Blonder & Michaletz, 2018).
- Megathermy occurs when T_c changes faster than T_a (slope > 1.1).
- True homeothermy occurs when T_c is nearly constant despite the variation in T_a (slope = 0). This is analogous to homeostasis as defined in the animal physiology literature (Billman, 2020).

Limited homeothermy occurs (1) when T_c changes slower than T_a (slope < 0.9) or (2) T_c is cooler than T_a at midday ($T_c < T_a$).

leading the T_c vs T_a regression slope to be < 1 (Fig. S1; Dong *et al.*, 2017; Blonder & Michaletz, 2018); (2) T_c is cooler than T_a when T_a exceeds some threshold, typically during high net radiation conditions (e.g. close to midday; Mahan & Upchurch, 1988). This is also called the 'limited homeothermy' hypothesis. Previously, this hypothesis was primarily tested using limited leaf-scale data in experimental conditions, such as glasshouse or gas change chambers, or on well-watered crop species (Still *et al.*, 2019; Farella *et al.*, 2022). However, whether such 'limited homeothermic' behaviors can be extended beyond the scale of individual leaves and whether it varies among different plant functional types (PFTs) around the world remains unknown.

In recent years, increasing observations from field surveys, experiments, eddy covariance (EC), and satellite remote sensing have been used to assess the spatial and temporal variability in T_c (Slot & Winter, 2017; Huang *et al.*, 2019; Guo *et al.*, 2022). However, debates remain, with diverse opinions ranging from no to moderate plant thermoregulation capability (Michaletz *et al.*, 2016; Blonder & Michaletz, 2018; Drake *et al.*, 2020). For example, the study by Drake *et al.* (2020) leveraged continuous measurements of T_c and T_a in *Eucalyptus parramattensis* tree canopies using a whole-tree chamber measurement technique and performed a series of analyses to assess T_c vs T_a relationships across a wide range of timescales from hourly to daily and weekly. Their results showed that T_c and T_a are tightly and linearly correlated, with their regression slopes close to 1 (poikilothermy, T_c changes almost at the same pace as T_a), regardless of the timescale analyzed, implying a surprising lack of thermoregulation of tree canopies across timescales, leading to the characterization of 'cold-blooded forests in a warming world' (Cavaleri, 2020).

However, previous studies have observed that plants exhibit thermoregulation capability, both temporally and spatially (Zeng *et al.*, 2017; Forzieri *et al.*, 2020). Based on an integration of global satellite-observed greenness and earth system models, the impact of the changing plant canopy structure on global-scale climate was assessed over the past three decades (Zeng *et al.*, 2017). This assessment indicated that the greening of the Earth (as indicated by the increase in leaf area index, LAI; Zhu *et al.*, 2016) helped to cool the Earth's surface temperature by 0.1°C, accounting for 20% of background global warming from 1982 to 2012, primarily due to the cooling benefit associated with the LAI-induced transpiration increase. Another satellite-based assessment also demonstrated that increasing LAI over decades had decreased sensible heat on vegetated surfaces, which is positively correlated with T_c–T_a difference (ΔT) (Forzieri *et al.*, 2020). These results imply that plants might not be as 'cold-blooded' as has sometimes been suggested (Cavaleri, 2020), as they can at least change their canopy structure to adapt to the warming planet.

Spatially, it has been widely shown that different PFTs and their specific key biophysical attributes (e.g. physiological traits and LAI) can often result in large differences in ΔT at the canopy and ecosystem scale (Leuzinger & Körner, 2007; Peng *et al.*, 2014; Duveiller *et al.*, 2018). For example, even within the same climate zone with comparable background climates, forests can cool down T_c by *c.* 1.1°C more than their neighboring croplands and grasslands (Peng *et al.*, 2014). Similar ΔT contrasts are also frequently observed in unhealthy vs healthy vegetation (Thakur *et al.*, 2021). Although ambient environments such as T_a and/or biotic variables such as LAI have been previously used to interpret spatial variability in ΔT (Lian *et al.*, 2017), whether other abiotic (e.g. wind speed and relative humidity (RH)) and biotic (e.g. PFT-specific physiological traits) factors that affect canopy transpiration also play a role in mediating T_c remains largely underexplored (Jones, 2013; Still *et al.*, 2021; Guo *et al.*, 2022), especially on a continental scale. Thus, a comprehensive assessment of large-scale variability in plant thermoregulation occurrence and capability is critically needed.

To resolve the above seemingly contrasting views and comprehensively evaluate the occurrence and degree of plant thermoregulation among various ecosystems, we addressed the following questions: (1) Across timescales (i.e. daily to weekly and monthly), to what extent does the 'limited homeothermy' hypothesis (i.e. slopes < 1 or midday $T_c < T_a$) hold? (2) Do its opposites (i.e. slope = 1 or midday $T_c > T_a$) imply no thermoregulation capacity? (3) Across global vegetated landscapes, do plant ecosystems display large spatial variation in ΔT and slope? and (4) What are the underlying biophysical mechanisms of spatial variability in ΔT and slope? To address these questions, we leveraged global datasets of T_c, T_a, other environmental variables derived from FLUXNET, Moderate Resolution Imaging Spectroradiometer (MODIS) satellite, and ERA5-Land (ERA5L) reanalysis data, and biotic variables approximated by satellite-derived LAI and PFTs maps, to evaluate the T_c vs T_a relationships on both temporal and spatial dimensions. Furthermore, we used generalized linear models and variance decomposition approaches to assess the relative effect of abiotic and biotic factors on the global plant thermoregulation variability.

Materials and Methods

Materials

Three types of data were used in this study, including (1) FLUXNET2015 (or EC) dataset of carbon and water fluxes

and meteorological variables; (2) globally available satellite products of land surface temperature (LST), land cover types, GPP, LAI, and PFTs; and (3) ERA5L products of key meteorological variables. Details of variables included in each data type, associated spatial/temporal resolutions, and access links are summarized in Table 1. FLUXNET2015 provides an important benchmark to assess temporal and spatial variation in T_c vs T_a relationships at the site scale, while the combined dataset of MODIS LST and ERA5L T_a provides a regional- to continental-scale assessment of T_c vs T_a relationships. Notably, EC- and satellite-based temperatures are surface temperatures of ecosystems, where plant canopies dominate if we restrict ecosystems/regions to pure vegetation areas during the growing seasons with dense LAI (threshold of $> 2.0\ m^2\ m^{-2}$, see details in 'Canopy temperature (T_c)' in the Materials and Methods section). We found good agreement between EC- and satellite-derived T_c (Fig. S2). Other environmental variables from ERA5L together with satellite-based PFTs and LAI were used to explore the proximate mechanisms underlying temporal and spatial variations in plant T_c. The detailed descriptions and relevant preprocessing of FLUXNET, satellite, and reanalysis data can be found in Methods S1, 1.1–1.3.

Tropical (20°N–20°S) and wetland regions (based on the IGBP classes) were excluded for the following reasons. The tropical regions were excluded because of the high cloud contamination of satellite data (Fig. S3) and the large uncertainty of the reanalysis data (Muñoz-Sabater *et al.*, 2021). We also present the EC-based results of tropical T_c vs T_a in Fig. S4, which are unimpacted by the above uncertainty, and they show very comparable findings to those derived from extratropical EC sites. The wetland regions were excluded because the T_c remote sensing products are often contaminated by underlying water bodies, and that can hinder accurate measurements (Wang *et al.*, 2019).

Methods

Our data analysis flowchart is summarized in Fig. S5 and includes four parts. First, to minimize the nongrowing season effect on the T_c vs T_a relationships, we focused our data analysis only on the growing season. Second, we extracted T_c from available EC and satellite measurements. Third, with paired measurements of T_c and T_a from either EC or satellite/ERA5L measurements, we analyzed the T_c vs T_a relationships in the temporal and spatial dimensions. Lastly, we used generalized linear modeling and variance decomposition approaches to explore the drivers of global plant thermoregulation variations.

Extraction of growing season data The growing season, defined as the period between the start (SOS) and the end (EOS) of the growing season each year, was extracted from global satellite phenology products (MODIS MCD12Q2) of 1 km resolution (Gray *et al.*, 2019). Specifically, SOS and EOS were calculated based on the seasonal cycle of enhanced vegetation index (Gray *et al.*, 2019). To assure high data quality, we first used the quality assurance (QA) band to filter out low-quality pixels and gap-filled empty pixels in the time series with multiple-year averages. For EC sites, their SOS and EOS were calculated as averages within a 3 × 3 pixel window centering around each site. Finally, all the EC, satellite, and ERA5L data outside of the growing season were filtered out.

Deriving T_c from EC and satellite measurements In this study, we focused on T_c vs T_a relationship during the time window

Table 1 Summary of the eddy covariance (EC) data, remote sensing data, and reanalysis data used in this study.

Variables	Definition	Unit	Resolutions (spatial/temporal)	Data source	References
T_{c_Aero}	Aerodynamic canopy temperature from EC data	°C	Site/hourly	FLUXNET	Pastorello *et al.* (2020)
T_{c_LW}	Radiative canopy temperature from EC data	°C	Site/hourly	FLUXNET	
T_{a_EC}	Air temperature from EC data	°C	Site/hourly	FLUXNET	
RH	Relative humidity from EC data	–	Site/hourly	FLUXNET	
u	Wind speed from EC data	$m\ s^{-1}$	Site/hourly	FLUXNET	
P	Precipitation from EC data	mm	Site/hourly	FLUXNET	
PAR	Photosynthetically active radiation from EC data	$W\ m^{-2}\ s^{-1}$	Site/hourly	FLUXNET	
T_{c_MODIS}	MODIS-derived canopy temperature	°C	1 km/8 d	MO(Y)D11A2	Wan (2014)
ESA-worldcover	Global land cover product at 10 m resolution for 2020	–	10 m/yearly	ESA/WorldCover	Zanaga *et al.* (2021)
IGBP map	PFT classification map	–	1 km/yearly	MCD12Q1	Friedl & Sulla-Menashe (2019)
SOS	Start of the growing season	DOY	500 m/yearly	MCD12Q2	Gray *et al.* (2019)
EOS	End of the growing season	DOY	500 m/yearly	MCD12Q2	
LAI	Leaf area index	$m^{-2}\ m^{-2}$	500 m/4 d	MCD15A3H	Myneni *et al.* (2015)
T_{a_ERA5L}	Near-surface air temperature from ERA5Land	°C	9 km/monthly	ERA5_Land	Muñoz-Sabater *et al.* (2021)
ϵ	Ecosystem surface emissivity	–	1 km/8 d	MOD21A2	Hulley *et al.* (2016)
W_{cov}	Waterbody coverage	%	30 m/yearly	JRC/GSW1_3	Pekel *et al.* (2016)

(10:00–14:00) close to midday for three reasons. First, this is consistent with previous studies, as the night-time T_c vs T_a relationship can be driven mainly by physical processes like longwave radiative cooling (although stomata still can open and regulate T_c vs T_a relationship at night, the extent of which remains largely uncertain; Sadok & Jagadish, 2020) and thus may not sufficiently reflect a plant canopy's thermoregulation capability (Mahan & Upchurch, 1988; Dong *et al.*, 2017). Second, the T_c vs T_a relationship at midday can best reflect thermoregulation differences between species or ecosystems since T_c variability induced by plant traits normally peaks at this time (Guo *et al.*, 2022). Third, this maintains consistency between EC and satellite observations, as MODIS satellites measure LST at *c.* 10:30 and 13:30 local time.

Canopy temperature (T_c). *Satellite-based T_c.* Satellite-based T_c was derived following three steps. Step 1 is the processing of MODIS LST products. The mean LST of day-time observations (at *c.* 10:30 and 13:30 local time) from the 8-d composited product (MOD&MYD11A2) was calculated to indicate satellite T_c. Low-quality pixels due to cloud contamination or emissivity estimation error were first filtered out with the product's QA band, and then, the missing pixels were gap-filled following the method by Zhou *et al.* (2021), which fills missing values based on the temporal information and has been demonstrated to have high accuracy.

Step 2 is filtering out all nonvegetation areas. For this, we first used the 10 m ESA WorldCover 2020 land cover map to generate the 1-km vegetation pixel fraction map following the methodology used in previous studies (Poulter *et al.*, 2015; Duveiller *et al.*, 2018), in which vegetation pixel fraction is defined as the ratio between vegetation pixels (tree, shrubland, grassland, and cropland) and all the pixels within each 1 km grid. We then filtered out all the pixels with vegetation pixel fraction < 95%.

Step 3 is filtering out sparse-vegetation areas (such as open shrubland with pure vegetation pixels but sparse-vegetation density) to minimize the effect of soil on LST. For this, we extracted the global LST, T_a, and LAI (from the MCD15A3H product) during the peak growing season in which the environmental conditions are similar for each pixel, and ΔT difference among pixels is mainly caused by soil fraction. We then plotted the points on a ΔT-LAI space and found that ΔT is sharply decreased with LAI increase (i.e. soil fraction decrease) when LAI is below 2 m^2 m^{-2} (Fig. S6a). Above 2 m^2 m^{-2}, ΔT only slightly decreases with LAI. However, after removing the effect of evapotranspiration (see Method S2), ΔT remains almost constant with LAI increases when LAI > 2 m^2 m^{-2} (Fig. S6b). The sensitivity analysis showed T_c vs T_a relationships were almost identical for LAI changes from 2.0 to 3.0 m^2 m^{-2} (Fig. S7). We finally selected the LAI threshold of 2.0 m^2 m^{-2} and filtered out pixels with mean growing season LAI < 2.0 m^2 m^{-2} and observations at the early or late growing season when corresponding LAI is < 2.0 m^2 m^{-2}. Furthermore, for the time-series data, extreme ΔT values (< 5 percentiles or > 95 percentiles) and corresponding LST and T_a were also filtered out as they were likely to be contaminated by nonvegetated backgrounds (Still *et al.*, 2021). Following these three steps, we derived the final LST maps of pure and dense vegetated canopies on the large scale, which were subsequently used for analyzing the T_c vs T_a relationships.

EC-based T_c. There are two widely used methods for deriving T_c from EC measurements, namely aerodynamic- (deriving aerodynamic T_c, T_{c_aero}; Eqn 1) and radiative-based (deriving longwave T_c, T_{c_LW}; Eqn 2) approaches (Doughty & Goulden, 2008; Campbell & Norman, 2012; Jones, 2013). In our analysis, we selected T_{c_aero} to indicate site-level T_c due to more T_{c_aero} data (146 sites remain after removing sparse-vegetation sites; Fig. 1) available than T_{c_LW} (94 sites) in FLUXNET2015, which ensured sufficient samples for each PFT. As an independent evaluation, we cross-compared the EC-derived T_{c_aero}, T_{c_LW}, and corresponding T_c vs T_a relationships. The results show that T_{c_aero} are highly consistent with T_{c_LW} (bias = 0.70, Pearson correlation = 0.93), and especially, when regressed against T_a,

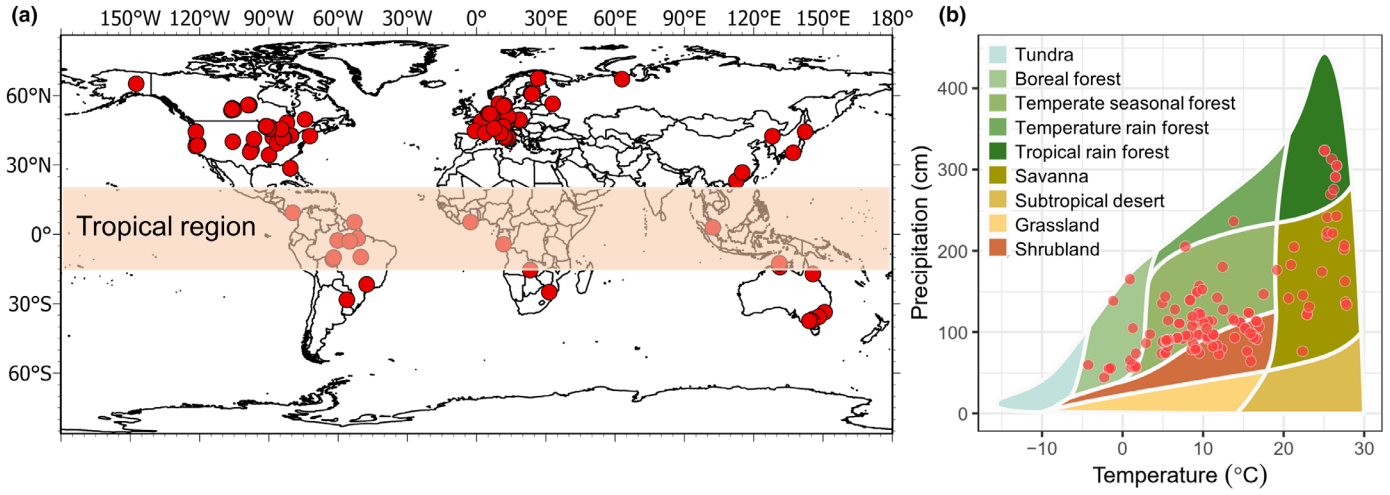

Fig. 1 Distribution of the flux sites from FLUXNET2015 shown as red circles (n = 146 sites including 965 site-year observations) world-wide. Location of each sampling site (a) on latitude and longitude grid and (b) on classic Whittaker Biome Classification by climate.

T_{c_aero} shows consistent patterns with T_{c_LW}, which is calculated completely independent of T_a (Fig. S8).

$$T_{c\_aero} = \left(\frac{u}{(u^*)^2} + 6.2u^{*-2/3}\right) \times \left(\frac{H}{c_p \rho_a}\right) + T_a \quad \text{Eqn 1}$$

$$T_{c\_LW} = \left[\frac{1}{\epsilon\sigma}\left(LW_{canopy} - (1-\epsilon)LW_{sky}\right)\right]^{1/4} \quad \text{Eqn 2}$$

where u is the horizontal wind speed (m s^{-1}), u^* is the friction velocity (m s^{-1}), H is the sensible heat flux (W m^{-2}), c_p is the specific heat capacity of air (= 29.3 J mol^{-1} K^{-1}), ρ_a is the density of wet air (kg m^3), ϵ is the emissivity (unitless) derived from MODIS emissivity product (MOD21A2), σ is the Stefan–Boltzmann constant (= 5.67×10^{-8} W m^{-2} K^{-4}), LW_{canopy} is the upward longwave radiation from the canopy surface (W m^{-2}), and LW_{sky} is the downward longwave radiation from the sky (W m^{-2}).

Matching the ERA5L T_a to the LST imaging time The imaging time of MODIS LST for different regions can differ by > 2 h across the globe (Fig. S9), which will lead to inaccurate comparisons of T_c and T_a if ignored. To avoid this, we matched the time between ERA5L T_a and MODIS LST pixel by pixel through three steps. First, we extracted the imaging time of LST of the Terra and Aqua sensors globally (Fig. S9; original accuracy: 0.1 h), and approximated them to the nearest half and hour. Second, we transformed the ERA5L T_a data from UTC to local solar time and then resampled T_a data from hourly to half-hourly by linear interpolation. Third, we paired the ERA5L T_a data with LST data based on their time labels pixel by pixel.

Assessing T_c vs T_a relationships To answer our Q1 (across daily to weekly and monthly timescales, to what extent does the 'limited homeothermy' hypothesis hold (i.e. T_c vs T_a slope < 1 and midday $T_c < T_a$, Box 1)), we assessed T_c vs T_a relationships based on temporal-scale regression. The regression slope ($\partial T_c / \partial T_a$), originally defined in Mahan & Upchurch (1988) and expanded in Michaletz *et al.* (2016) and Drake *et al.* (2020), has been widely used because it has clear implications for plant thermoregulation (Box 1). In addition to the slope, the midday ($T_c - T_a$) difference was also used. It was hypothesized that under sufficiently high net radiation situations (e.g. midday), a sufficiently high transpiration rate would help cool T_c below T_a (i.e. $T_c < T_a$ at midday) to maintain T_c closer to the optimal photosynthesis temperature and avoid damaging temperature extremes (Linacre, 1964; Mahan & Upchurch, 1988; Blonder *et al.*, 2020).

We conducted a temporal evaluation of the T_c vs T_a relationships at the EC site level covering the timescale of daily (i.e. measurements aggregated to daily averages), weekly, and monthly (i.e. daily averages are aggregated to weekly and monthly mean) observations. There are two reasons for covering different timescales. First, the degree of the coupling between meteorological variables (e.g. temperatures) is often affected by timescales (Novick *et al.*, 2016), and T_c vs T_a relationship may also be affected by this but remains unexplored. Second, the different timescale analyses can help assess the consistency of results from the measurements with different temporal resolutions, such as ground-based (flux site: sub-daily) and satellite-based (weekly to monthly) observations. For each satellite pixel, a single slope across all months over the 10 yr was calculated.

To answer our Q2 (Do the opposites of limited homeothermy hypothesis (i.e. slope = 1; midday $T_c > T_a$) imply no thermoregulation capability?), we conducted two analyses. First, to explore whether slope ≥ 1 is equal to no thermoregulation, we focused on the temporal partial correlations between plant structure variable (LAI), climate, and ΔT. We expected that if ΔT fluctuates nonrandomly following certain seasonal patterns, and these patterns are related to the intrinsic seasonal change in the plants such as structural changes measured by LAI, this would suggest that plants do exhibit thermoregulation across the seasonal timescale, even if the slopes are ≥ 1. Specifically, we plotted the seasonal pattern of ΔT for each site and performed time-series randomness analysis (with the 'runs.test' R package; Gibbons & Chakraborti, 2014) to assess whether ΔT variability is random across the growing season. Additionally, we also conducted a partial correlation analysis between ΔT and LAI phenology for each site (partial correlation analysis was selected to minimize the impact of high correlation among LAI phenology and environmental variables, such as photosynthetically active radiation (PAR) and precipitation, Fig. S10), and then calculated the percentage of global sites that showed significant partial correlations between ΔT seasonality and LAI phenology.

Second, to explore whether midday $T_c > T_a$ implies no thermoregulation, we compared the relationship between T_a, T_c, and soil temperature (T_s, no thermoregulation capacity) based on the Breathing Earth System Simulator (BESS) model simulation (Ryu *et al.*, 2011) following the method of Guo *et al.* (2022). Notably, T_s was simulated at the same conditions as the canopies. We expected that if thermoregulation occurs, T_c will exhibit obvious variability among the different trait combinations. Meanwhile, since the soil surface has no thermoregulation, we would also expect that T_c will be cooler than T_s.

To answer our Q3 (Across global vegetated landscapes, do plant canopies display large spatial variation in ΔT?), we assessed how ΔT varied across global vegetated landscapes. Specifically, we calculated ΔT for each EC site/satellite pixel over entire growing seasons and then derived the mean and standard deviation of ΔT for each biome type.

Exploring the drivers of global variation in plant thermoregulation To answer our Q4 (What are the underlying biophysical mechanisms of spatial variability in ΔT and slope?), we used generalized linear models. In this analysis, nine abiotic and biotic factors from FLUXNET, satellite, or reanalysis product (Table 1), including T_a, elevation, wind speed (u), RH, vapor pressure deficit (VPD), solar radiation (PAR), LAI, precipitation (P), and PFTs that show direct linkages with plant energy balance, were used as the explanatory variables. To minimize collinearity among these factors, we calculated their pairwise Pearson

correlation coefficients and found that VPD was highly correlated with T_a ($r = 0.68$) and RH ($r = 0.72$). We thus removed VPD from the following analysis. The remaining variables exhibited Pearson correlations of $r < 0.7$ (Fig. S11).

This analysis was conducted for both EC and satellite data, including four steps. First was variable normalization. All variables were standardized using the *Z*-score approach (García-Palacios *et al.*, 2018). Second, the standardized variables were used to build the generalized linear models. In the initial model analysis, all abiotic variables, biotic variables, and interactions between abiotic and biotic factors were considered. The interactions included 10 one-by-one combinations (i.e. T_a/P/PAR/elevation/RH by LAI/PFTs; the interaction between wind speed and LAI/PFTs was excluded due to lacking obvious linkage among them; Iio *et al.*, 2014; Fang *et al.*, 2019). Third was model optimization and validation. We used the Akaike information criterion (AIC) to select the optimal model ('step' function in R), with smaller AICs indicating better models (Zuur *et al.*, 2009). As a result, the eight independent factors (T_a, elevation, wind speed, P, RH, PAR, LAI, and PFT) and six interactions (T_a/P/PAR by LAI/PFT) were identified and used in the final model (Table S1). Thereafter, we checked the homogeneity and normality of the model residuals to validate the model assumptions (Figs S12, S13). Finally, we used the variance decomposition method (García-Palacios *et al.*, 2018) to assess the effect of each factor on ΔT and slope variability.

Results

Assessing the occurrence of limited thermoregulation behaviors across temporal scales

Using the slope indicator, plant ecosystems show diverse thermoregulation strategies globally (from homeothermic to poikilothermic and megathermic), while midday T_c is consistently higher than T_a, disagreeing with the homeothermic hypothesis as originally proposed by Mahan & Upchurch (1988). Specifically, our results from both EC and satellite measurements show that T_c and T_a are tightly and linearly correlated across all the timescales examined, and slope indicators for most global vegetated sites/areas varied from 0.7 to 1.3 (Figs 2, 3). For the EC-derived relationship between T_c and T_a, we observed that the slope indicator of most EC sites is > 0.9 (i.e. poikilothermic or megathermic), including 95% of all sites on the daily timescale, 94% of sites on the weekly timescale, and 94% of sites on the monthly timescale (Fig. 2). Meanwhile, among these analyses, we also observed very high predictive powers of T_a for explaining T_c variability, with an average R^2 of 0.94 for daily, 0.95 for weekly, and 0.95 for monthly data (Fig. 2). When moving from the EC site-scale analysis to satellite global-scale analysis, global vegetated areas have a mean slope of 0.97 with 68% > 0.9 (Fig. 3b), and the amount of T_a explaining T_c variability across time is 0.83 (Fig. 3c).

From the regression panels (Figs 2, 3a), almost all the scatter points are located above the 1 : 1 line, indicating midday T_c is generally warmer than surrounding air, which disagrees with the original limited homeothermy hypothesis that argues midday T_c is cooler than T_a (Mahan & Upchurch, 1988).

The opposites of limited homeothermic conditions

Our results show that for the sites with a slope ≥ 1, their ΔT follows certain patterns rather than varying randomly over the growing seasons (Fig. 4). Specifically, ΔT displays a tight correlation with climate and LAI seasonality (Fig. S10). When removing the site-climate seasonality effect, 84% of global EC sites show significant negative partial correlations of LAI phenology on ΔT seasonality (Fig. 4b), even for the sites with slope close to 1 (Fig. 4c, d; traditionally considered as no thermoregulation). In other words, ΔT declines as LAI increases at the seasonal timescale for most sites. This indicates that passive and structurally driven plant thermoregulation can vary considerably over the seasons for most global vegetated sites/areas, and LAI (together with climate) seasonality explains the observed seasonal thermoregulation variations.

We compared the differences between T_c, T_a, and T_s based on simulations of the BESS model (Fig. 5). Regardless of background climate and PFTs, our results show that T_c is consistently warmer than T_a but cooler than T_s at midday of the peak growing season. This indicates that plant ecosystems still exhibit thermoregulation capability when $T_c > T_a$ at midday, as they are cooler than objects without thermoregulation (soil surface). Furthermore, our simulated results show that different plant species (represented by the different trait combinations) exhibit different T_c in the same environment, with a lower ΔT indicating higher transpiration cooling and thus higher thermoregulation capacity. These results together demonstrate that traditional widely used standards (i.e. slope < 1 or midday $T_c < T_a$) are sufficient but not necessary conditions for thermoregulation, since thermoregulation still can occur even when the slope > 1 or midday $T_c > T_a$.

Assessing T_c vs T_a relationships across global vegetated landscapes

Regardless of the use of either site-level EC or larger scale satellite datasets, our results consistently show that vegetated ecosystems display considerable thermoregulation variations across global vegetated sites and PFTs (Figs 3, 6, 7). Like the slope indicator (Fig. 3), ΔT also displays considerable spatial variability in the range of 0–6°C (Fig. 6a,b), implying thermoregulation differences globally. When aggregating the value from each site or pixel to the PFT level, both ΔT and slope display considerable variations among PFTs (Fig. 7). Specifically, savanna, shrubland, grassland, and cropland generally exhibit higher ΔT than broadleaf, needleleaf, and mixed forests (Fig. 7a,b), implying forest ecosystems may have higher thermoregulation capability than the other vegetated ecosystems.

Meanwhile, slope indicators also exhibit a significant difference between PFTs (Fig. 7c,d), but their variance is smaller than that of ΔT, as indicated by the coefficient of variance (cv) of ΔT (cv = 0.25; Fig. 7b) being three times that of slope indicators

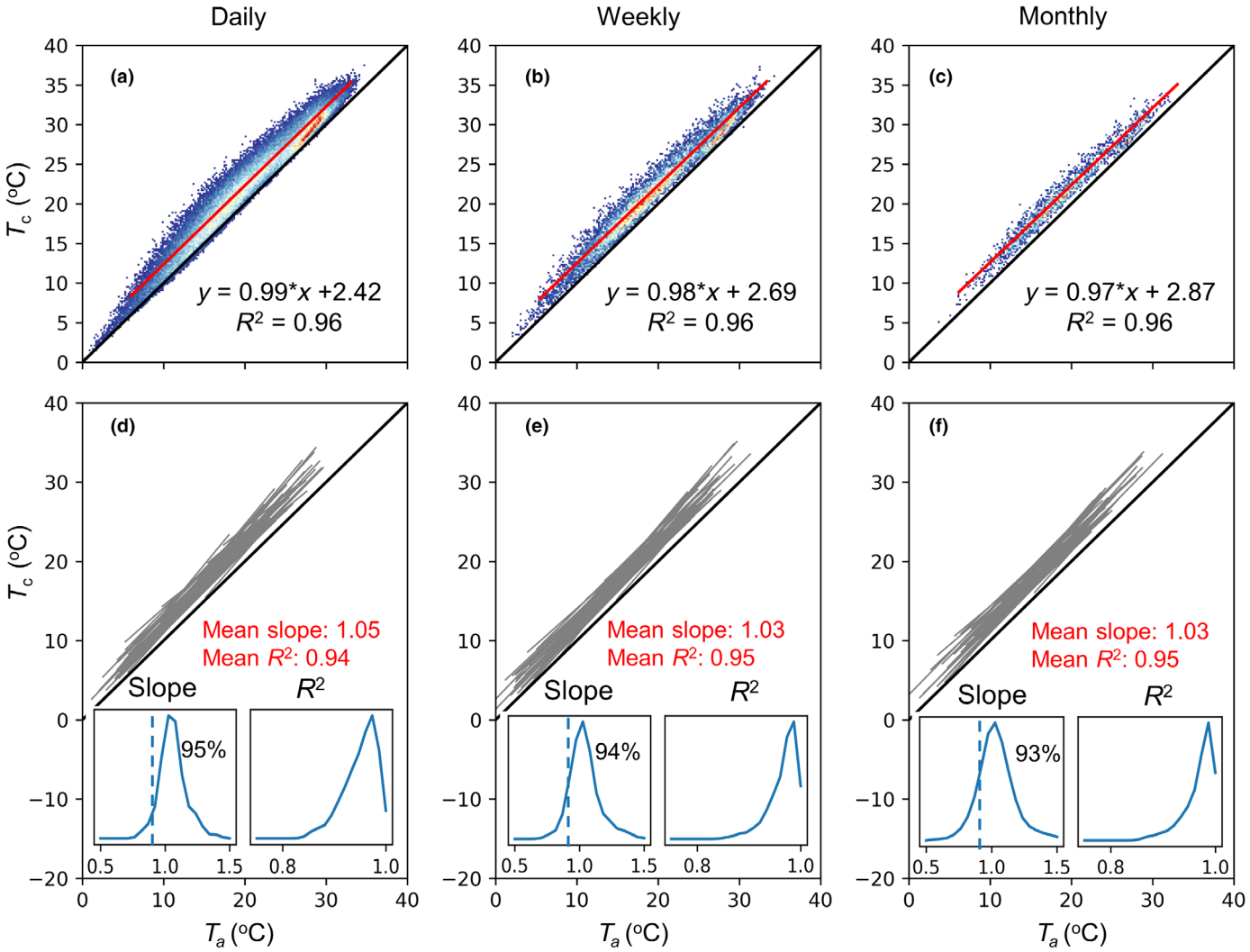

Fig. 2 Temporal-scale regressions of canopy temperature (T_c) vs air temperature (T_a) across daily, weekly, and monthly timescales using EC data. (a–c) Fitted results of T_c vs T_a derived from data across all available sites ($n = 144$). (d–f) Fitted results of T_c vs T_a for each EC site, where each gray line corresponds to each site. Histograms indicate frequency distributions of regression slope and R^2, the blue dashed line is the slope = 0.9, and the number is the percent of slope > 0.9.

(cv = 0.08; Fig. 7d), suggesting that ΔT is more sensitive to distinguishing the thermoregulation difference between PFTs than the slope indicator.

Drivers of spatial variations in plant thermoregulation

Our results from both EC and satellite measurements (Fig. 8a,b) show that the eight abiotic and biotic factors, combined with their interactions, jointly explain 53% or 61% of the spatial variability of ΔT, in which abiotic factors dominate, followed by biotic factors and interaction terms. Specifically, three abiotic factors are positively correlated with spatial variability of ΔT: PAR, elevation, and RH; three are negatively correlated with ΔT: T_a, wind speed, and precipitation. For the biotic factors, both LAI and PFTs show significant relationships with ΔT. The interactions between abiotic and biotic factors, including $T_a \times$ LAI, PAR × LAI, precipitation × LAI, $T_a \times$ PFTs, and PAR × PFTs, also show significant relationships with ΔT (Table S2).

Meanwhile, our results (Fig. S14) from both EC and satellite measurements show that the eight abiotic and biotic factors combined with their interactions provide a low explanation for the global regression slope variability ($R^2 = 0.26$ for EC data and $R^2 = 0.21$ for satellite data).

Discussion

Do plants show thermoregulation at the temporal scale?

Whether plants can thermoregulate themselves to adapt to future warming climates has received increasing attention over recent years, but remains debated with views from no to moderate thermoregulation capabilities (Farella *et al.*, 2022; Still *et al.*, 2022). To reconcile these seemingly contrasting views, we assessed the extent to which the 'limited homeothermy' hypothesis holds across various plant ecosystems. Our results show that there is moderate variation in regression slopes of T_c vs T_a across global

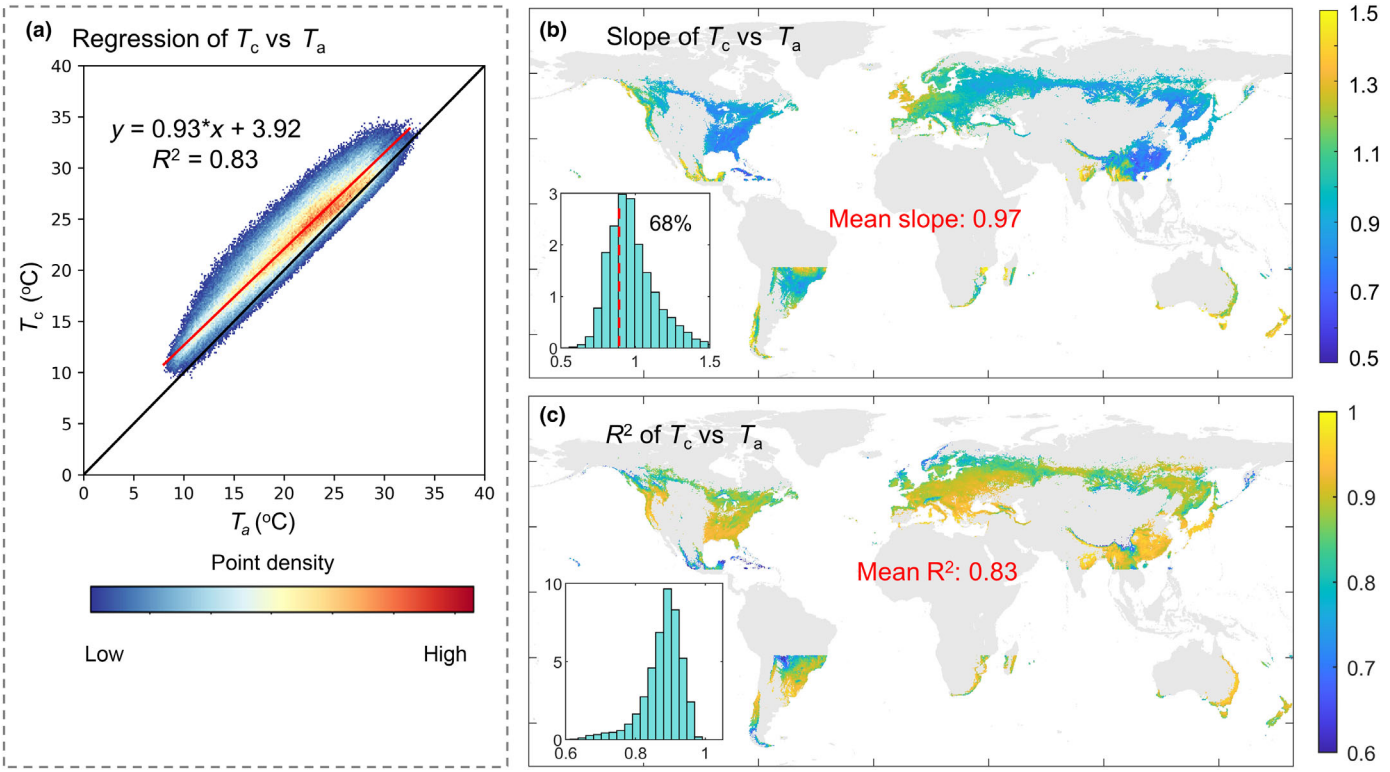

Fig. 3 Temporal regressions of canopy temperature (T_c) vs air temperature (T_a) at 8-d timescales using satellite (or RS) data. (a) Fitted result of T_c vs T_a from dense vegetated satellite pixels (defined by vegetation cover > 95% and leaf area index > 2.0 m^2 m^{-2}, see details in 'Canopy temperature (T_c)' in the Materials and Methods section); (b) slope (unitless) of T_c vs T_a; (c) R^2 (unitless) of T_c vs T_a. The red dashed line is the slope = 0.9, and the number is the percent of slope > 0.9.

vegetated sites/areas, regardless of the timescales (from daily to weekly and monthly) examined, or the data (EC vs satellite) used (Figs 1–3). These results suggest that the plant thermoregulation patterns are diverse across global vegetated sites/areas, ranging from limited homeothermy (slope < 0.9) to poikilothermy (slope: 0.9–1.1) and megathermy (slope > 1.1), but the large majority (*c.* 80%) of our data with slope > 0.9 indicate that poikilothermy and megathermy are by far the dominant patterns. Furthermore, this may suggest that divergent conclusions (no vs moderate thermoregulation capacities) from prior studies may not be incompatible and are likely because different studies were conducted in different biomes and under different biotic and abiotic conditions.

After testing the 'limited homeothermy' hypothesis across global extratropics, we next explored whether its opposites (slope < 1 or $T_c < T_a$ at midday) are the same as no thermoregulation capability as interpreted previously (Cavaleri, 2020). To this end, we explored seasonal fluctuations of ΔT, and assessed their partial correlations with LAI phenology. The hypothesis here is that if there is little-to-no thermoregulation capability at the temporal scale, we would expect random fluctuations of ΔT across the season. By contrast, our results show that there are considerable seasonal dynamics in ΔT that tightly follow climate seasonality and/or LAI dynamics (Fig. S10). Further analysis shows that when removing the effect associated with site-specific climate seasonality, we observed 84% of EC sites showing significant negative impacts of LAI in regulating ΔT seasonality (Figs 4, S10, S15), including those sites with slopes ≥ 1. In other words, even when the slope is ≥ 1, plants are not as 'cold-blood' as interpreted previously. In addition to the regression slope, midday ΔT was also used for hypothesis testing. Contrasting to the expectation, over 96% of global extratropical ecosystems display positive values of midday ΔT, rejecting the hypothesis. Such observed positive midday ΔT results from the interactive consequence of high solar radiation and plant thermoregulation (Blonder *et al.*, 2020; Still *et al.*, 2021; Guo *et al.*, 2022), which was further confirmed by the process modeling results. Specifically, our results from the BESS model show that the soil with no thermoregulation capability exhibits a much higher positive ΔT than plants (Fig. 5), supporting the occurrence of plant thermoregulation even when $T_c > T_a$ around midday. The slope indicator together with ΔT depicts a more comprehensive picture of plant thermoregulation occurrence and strategies.

The finding of significant correlations between the seasonalities in ΔT, climate, and LAI (Fig. 4) also sheds critical insights into the processes and mechanisms underlying plant thermoregulation. First, consistent with previous empirical and modeling studies (Campbell & Norman, 2012; Jones, 2013; Perera *et al.*, 2019), our results show that T_a is the first-order control of temporal variability in T_c and explains *c.* 90% of its variation. When minimizing the influence of background T_a and focusing on the seasonal dynamics in ΔT, other climatic variables, such as PAR, wind speed, and RH (Fig. S10), start to exhibit their roles in influencing ΔT seasonality. Thus, ΔT is a more sensitive

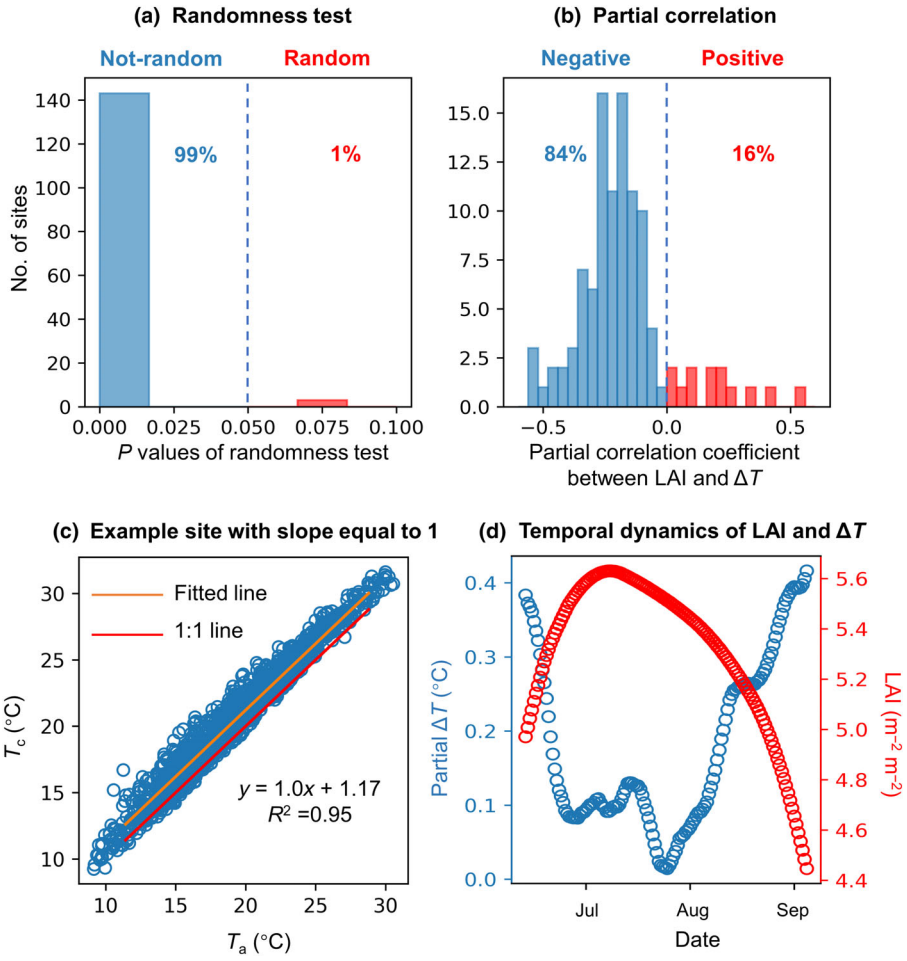

Fig. 4 Temporal dynamics of canopy-to-air temperature difference (ΔT) and its relationship with the seasonality of leaf area index (LAI). (a) Randomness test of temporal ΔT for each eddy covariance (EC) site. (b) Partial correlation analysis between the seasonalities of LAI and ΔT for each EC site, in which the influence of air temperature, relative humidity, PAR, and wind speed was controlled. (c, d) An example EC site (FR-Fon: mixed forest) with a regression slope of 1.0, where ΔT seasonality follows a regular pattern and is negatively partially correlated with LAI. Temporal ΔT and LAI are smoothed with a 10-d window.

indicator to detect temporal variability of plant thermoregulation than raw T_c.

What are the mechanisms underlying large spatial variation in plant thermoregulation capability?

Our results from both EC and satellite measurements consistently demonstrate large variations in plant thermoregulation capability (indicated by ΔT) across PFTs, following the descending order of ΔT (ascending thermoregulation capability): grassland, shrubland, savanna, cropland, and forest (Fig. 7). Such observations are also consistent with many previous findings respectively made using EC (Duman *et al.*, 2021; Javadian *et al.*, 2022), proximate remote sensing (Still *et al.*, 2021; Yang *et al.*, 2021), and satellite (Lian *et al.*, 2017; Duveiller *et al.*, 2018) measurements. The widespread presence of ΔT variability further suggests that the conventional approach of using T_a alone for inferring T_c could produce large uncertainty.

However, challenges remain in understanding the relative role of abiotic and biotic factors in driving large spatial variations in ΔT. Therefore, we performed a holistic assessment to explore the underlying biophysical mechanisms of ΔT variations. Our results demonstrate that ΔT variability across global extratropics is explained primarily by abiotic factors (24–38%) and secondarily by biotic factors (14–15%; Fig. 8). This result is new as it is for the first time explored here based on large-scale datasets. Our findings also agree with fundamental ecophysiological and biophysical principles. For example, we observed T_a and RH as the two important variables correlated with ΔT, which is because T_a and RH jointly affect atmospheric VPD that shows direct connections with stomatal conductance and canopy transpiration, thus importantly regulating ΔT (Ahi *et al.*, 2015; Medina *et al.*, 2019). We also observed a positive relationship of PAR-ΔT, which is primarily because higher PAR means more solar radiation absorbed by plant canopies, which could subsequently raise T_c, causing a higher ΔT (Gates, 1965; Jones, 2013; Fauset *et al.*, 2018). In addition, we observed a significant, negative relationship between elevation and ΔT. The underlying explanation might be related to leaf size, which has been shown to decrease with elevation, and the smaller leaf size often leads to an increase in boundary layer conductance and thus a smaller ΔT at the higher elevation (Wright *et al.*, 2017; Guo *et al.*, 2022).

Moreover, we used the PFT variable to approximate the factors related to biotic regulations, as many global-scale studies have shown that key physiological and morphological traits can vary considerably across PFTs (Kattge *et al.*, 2011; Anderegg *et al.*, 2021). We found that PFT indeed exerted a considerable role in regulating ΔT variations (Figs 7, 8) as we hypothesized. Despite

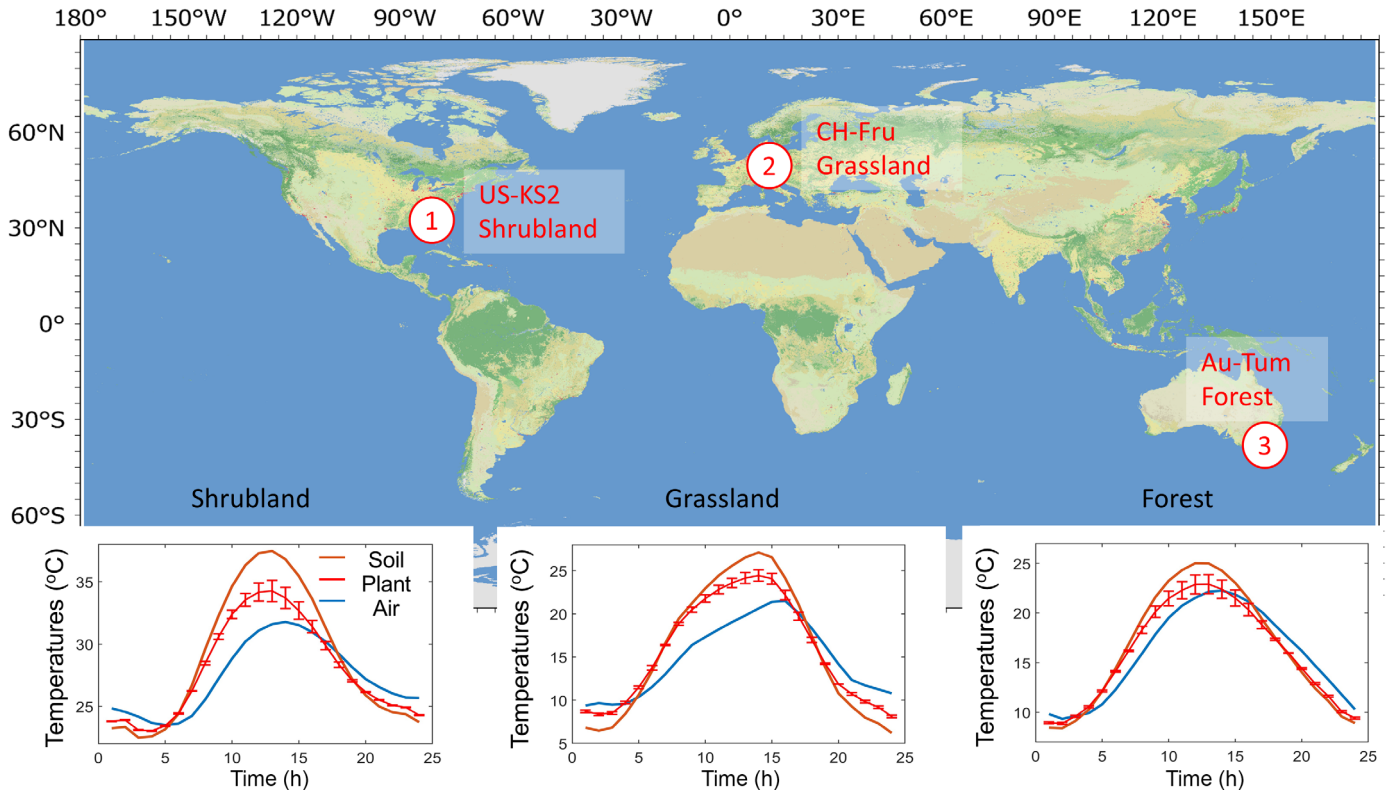

Fig. 5 Comparison between simulated canopy temperature (T_c), air temperature (T_a), and soil temperature (T_s) from the Breathing Earth System Simulator model. The input climate data are from three sites: (1) US-KS2 shrubland (mean of 2003-2007), (2) CH-Fru grassland (mean of 2008-2007), and (3) AU-Tum forest (mean of 2008-2001). The input trait data are from Guo *et al*. (2022). The error bar indicates the 1.5× SD and refers to T_c variability induced by the traits.

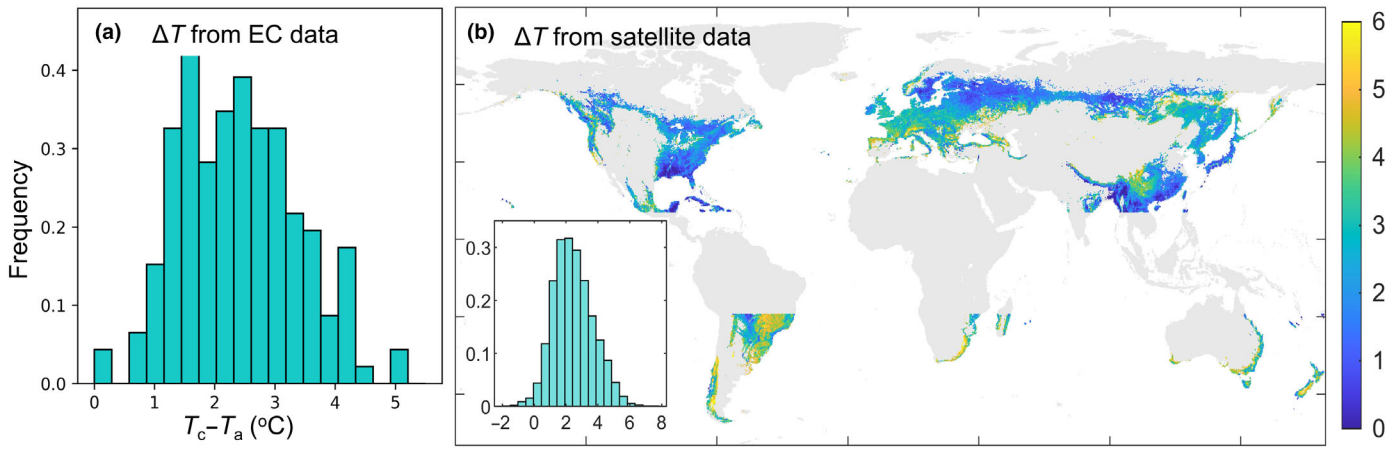

Fig. 6 Eddy covariance (EC)- and satellite-based canopy-to-air temperature differences (ΔT) across the global vegetated landscape. (a) Histogram of EC-based ΔT. (b) Satellite-based ΔT (°C).

this, we also observed large ΔT variation within each PFT (Fig. 7), which could largely be attributed to the insufficient approximate of PFT for plant physiological traits, as many fine-scale studies have documented large trait variations within the same PFT (Kattge *et al*., 2011; Wu *et al*., 2019). These results suggest that variations in key plant physiological and morphological traits (e.g. leaf size, stomata slope, and maximum carboxylation rate, Guo *et al*., 2022) can largely affect plant thermoregulation. Meanwhile, it also highlights that a comprehensive set of field-measured plant traits might play an even greater role in interpreting the biotic regulation of ΔT than currently captured by the PFT variable used in this study.

Lastly, this study for the first time systematically compared the performances of ΔT and slope as thermoregulation indicators on a large scale, highlighting there would be condition-specific preference for each of the two thermoregulation indicators. For

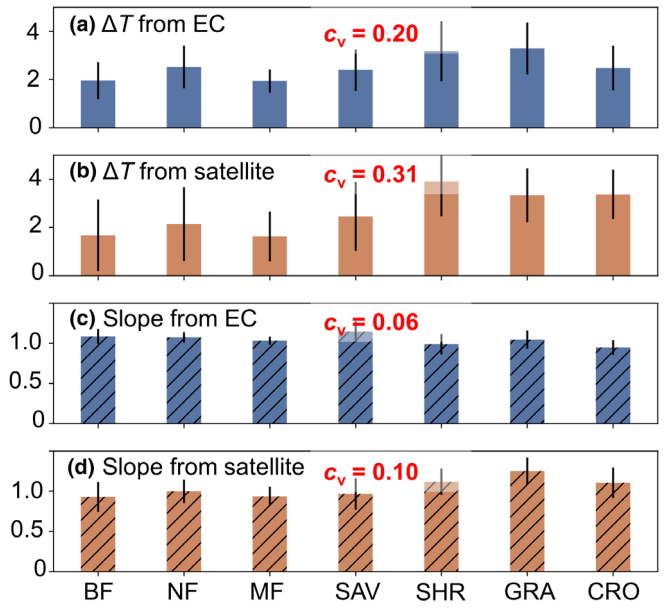

Fig. 7 Canopy-to-air temperature difference (ΔT) and slope indicator (weekly timescale) grouped by plant functional types (PFTs). (a) Eddy covariance (EC)-based ΔT; (b) satellite-based ΔT; (c) EC-based slope indicator; (d) satellite-based slope indicator. BF, broadleaved forest; CRO, cropland; GRA, grassland; MF, mixed forest; NF, needle-leaved forest; SAV, savanna; SHR, shrubland. Error bar indicates 1.5× SD.

example, as shown in Fig. 8, ΔT varies considerably across different PFTs, but the slope indicator is indistinguishable (Fig. 8). These findings thus suggest that ΔT could be a more suitable metric for studying the influence of vegetation change, such as deforestation or afforestation (Duveiller *et al.*, 2018; Zeng *et al.*, 2021), on T_c and other associated ecophysiological processes, as the ΔT indicator can easily distinguish the thermoregulation difference between different PFTs. On the contrary, the slope indicator that quantifies the relative change speed between T_c and T_a over time could be more insightful when projecting the thermal response of plants to the future climate condition (Dong *et al.*, 2017; Blonder & Michaletz, 2018), but the long-term accurate ground data are needed to verify this implication.

Caveats and future directions

Our work identifies three important caveats that require further research. First is data uncertainty. Despite a vastly large spatial coverage, T_a, T_c, and LAI measurements from reanalysis and satellite products come with larger uncertainties than ground-based observations (e.g. EC data or field-measured LAI). These unavoidable uncertainties are results of the inherent bias in reanalysis systems and the effect of sensor noises and unstable atmospheric conditions in satellite-based retrievals (Wan, 2014; Parker, 2016; Muñoz-Sabater *et al.*, 2021). Additionally, due to the coarse resolution, T_c from satellite or EC cannot eliminate interference from nonleaf information, such as branches and trunks (Farella *et al.*, 2022). Furthermore, both EC- and satellite-derived T_c mainly reflect the dynamics of the upper canopies and rarely reflect the T_c of middle canopies or understory (Still *et al.*, 2021). Despite these limitations, our study has important implications for ecology, since upper canopies contribute a very large

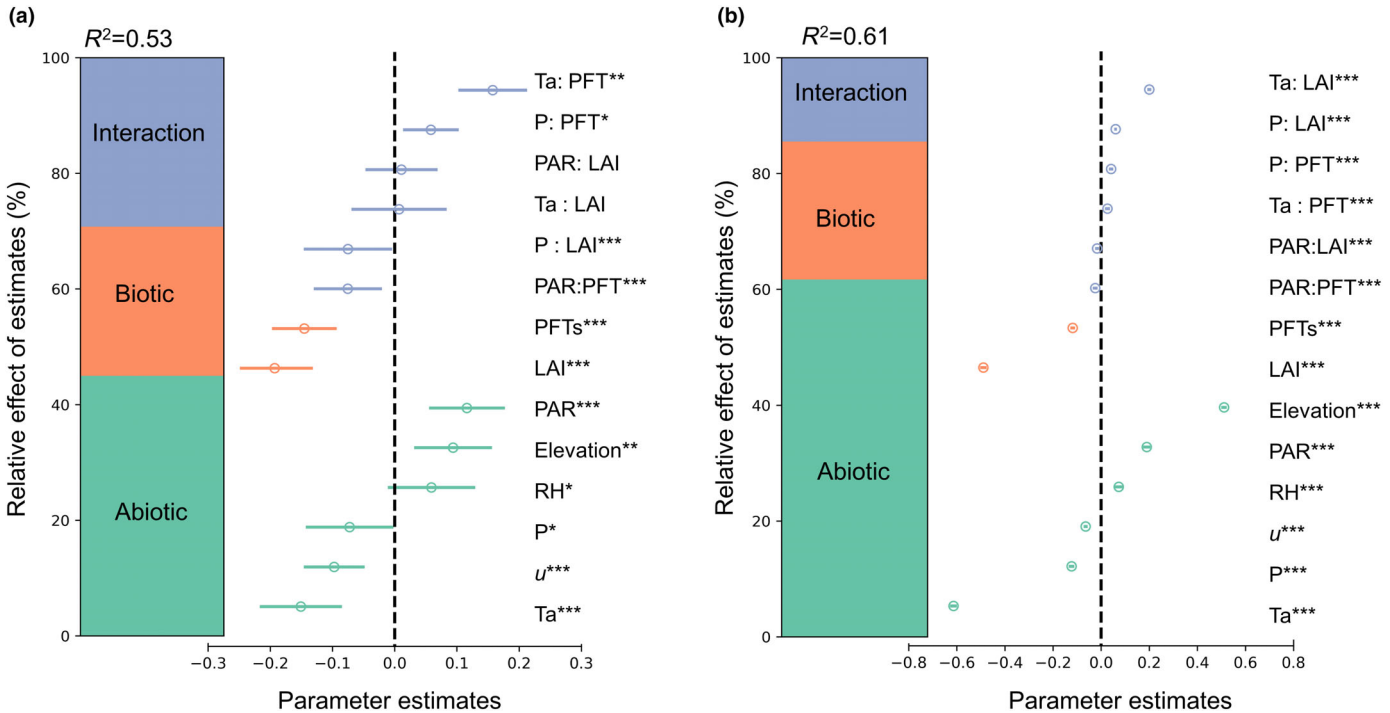

Fig. 8 Relative importance of the eight selected abiotic and biotic factors for explaining global variability in the original canopy-to-air temperature difference (ΔT). (a) Eddy covariance-based results. (b) Satellite-based results. In both figures, the circle is the mean value, and the error bar indicates 1.5× SD. The relative effect is calculated based on standardized variables. LAI, leaf area index; *P*, precipitation; PAR, photosynthetically active radiation; PFTs, plant functional types; RH, relative humidity; T_a, air temperature; *u*, wind speed. *, $P < 0.05$; **, $P < 0.01$; ***, $P < 0.001$.

amount of carbon and water fluxes compared with the middle canopy and understory (Ellsworth & Reich, 1993). Other important physiological and morphological traits, such as leaf size and stomatal slope, shown to be tightly linked to ΔT (Guo *et al.*, 2022), were not explored due to data limitations. Future attempts that leverage detailed traits by field measurements (e.g. Blonder *et al.*, 2020; Yan *et al.*, 2021) or imaging spectroscopy techniques (Kattenborn *et al.*, 2019; Wu *et al.*, 2021) are needed to comprehensively assess the role of these important biotic components in plant thermoregulation.

Second, our current exploration of the biophysical mechanisms underlying plant thermoregulation is based on a generalized linear model. This approach served well for our work, but is not process-based (García-Palacios *et al.*, 2018), thus cannot be directly implemented in large-scale process-based models (e.g. terrestrial biosphere models, TBMs) for simulating T_c and associated key ecophysiological processes (Ryu *et al.*, 2011). Thus, an important next step is leveraging detailed field measurements to first evaluate TBMs and see whether the mechanisms revealed in this paper hold in the TBMs and then assess the potential impacts of with/without thermoregulation-related mechanisms on larger scale simulations of ecosystem responses to climate change.

Finally, our EC- and satellite-based findings of the magnitude of day-time ΔT variation (0–6°C) and associated underlying biotic importance (15–25%) are smaller than previous observations made on the leaf and canopy scale (Ehleringer *et al.*, 1976; Smith & Carter, 1988; Guo *et al.*, 2022). This can be caused by the effect of canopy structure (e.g. self-shading and canopy gaps) and microclimate, but has not been explored comprehensively (Pau *et al.*, 2018; Javadian *et al.*, 2022). Thus, it is reasonable to expect that there are scale-dependent mechanisms in regulating plant thermoregulation capability. In future attempts, a holistic set of measurements covering scales from single leaves to plant canopies and ecosystems remain needed to reveal more detailed scale-dependent mechanisms and improve the understanding of diverse plant thermoregulation strategies across various scales.

Conclusion

In this study, we tested the limited homeothermy hypothesis for various plant ecosystems across space and time, and explored the drivers of large-scale plant thermoregulation variability. Temporally, our results show that *c.* 90% of the slope indicators vary from 0.7 to 1.3, suggesting that diverse thermoregulation strategies occur for plants globally. While, even for the poikilothermic or megathermy sites, their ΔT exhibits regular seasonal variations, which show negative, partial correlations with canopy structure dynamic. Spatially, our results show that midday ΔT exhibits large variations across global extratropics and almost all values are positive, which contradicts the 'homeothermic cooling' at higher temperatures as originally proposed by Mahan & Upchurch (1988). These results suggest slope < 1 or $T_c < T_a$ at midday are not necessary conditions for plant thermoregulation, as thermoregulation still occurs in their opposite (i.e. slope ≥ 1 or $T_c > T_a$). Furthermore, we found that abiotic and biotic drivers (T_a, PAR, RH, elevation, precipitation, wind speed, LAI, and PFTs), combined with the interaction terms, jointly explained 53–61% of large spatial-wide ΔT variations across global extratropics (Fig. 8), among which abiotic factors dominated. These results altogether thus improve our understanding of plant thermoregulation occurrence and capability across both space and time, highlighting the fundamental biophysical mechanisms underlying diverse plant thermoregulation strategies around the world.

Acknowledgements

We thank Prof. Jin Chen and Mr. Bartosz M. Majcher for their constructive suggestions and kind help on the manuscript. This work was supported by the National Natural Science Foundation of China (no. 31922090), Hong Kong Research Grants Council Early Career Scheme (no. 27306020). JW was in part supported by the Innovation and Technology Fund (funding support to State Key Laboratories in Hong Kong of Agrobiotechnology) of the HKSAR, China. CJS was supported by the US National Science Foundation (awards 1802885 and 1926431). CKFL was in part supported by the HKU Seed Fund for Basic Research (no. 202011159154) and the HKU 45th round PDF scheme.

Competing interests

None declared.

Author contributions

ZG and J Wu conceived the study and wrote the manuscript with inputs from all authors. ZG designed the analyses with inputs from CJS and J Wu. ZG performed the analyses. ZG, CJS, CKFL, YR, BB, J Wang, YL and J Wu contributed to interpreting the results. TCB, AH, HCHY, KZ, YKL and ZL contributed to writing the manuscript.

ORCID

Benjamin Blonder https://orcid.org/0000-0002-5061-2385
Zhengfei Guo https://orcid.org/0000-0001-8806-1307
Alice Hughes https://orcid.org/0000-0002-4899-3158
Youngryel Ryu https://orcid.org/0000-0001-6238-2479
Christopher J. Still https://orcid.org/0000-0002-8295-4494
Jin Wu https://orcid.org/0000-0001-8991-3970

Data availability

FLUXNET 2015 data are available at https://fluxnet.org/data/fluxnet2015-dataset/subset-data-product/, the MODIS LST data are available at https://lpdaac.usgs.gov/products/myd11a2v006/ and https://lpdaac.usgs.gov/products/mod11a2v006/, the MODIS emissivity data are available at https://lpdaac.usgs.gov/products/mod21a2v006/, the ESA-worldcover data are available at https://viewer.esa-worldcover.org/worldcover/, the MODIS IGBP map is available at https://lpdaac.usgs.gov/products/mcd12q1v006/, the MODIS phenology data (i.e. SOS and EOS) are available at https://lpdaac.usgs.gov/products/mcd12q2v006/, the MODIS LAI

data are available at https://lpdaac.usgs.gov/products/mcd15a3hv006/, the ERA5_Land data are available at https://www.ecmwf.int/en/era5-land, and the water body coverage data are available at https://global-surface-water.appspot.com/download. The codes for the analyses are available at https://github.com/guozhengfei/Global-thermoregulation-evaluation.

References

Ahi Y, Orta H, Gündüz A, Gültaş HT. 2015. The canopy temperature response to vapor pressure deficit of grapevine cv. Semillon and Razaki. *Agriculture and Agricultural Science Procedia* **4**: 399–407.

Anderegg LD, Griffith DM, Cavender-Bares J, Riley WJ, Berry JA, Dawson TE, Still CJ. 2021. Representing plant diversity in land models: an evolutionary approach to make "Functional Types" more functional. *Global Change Biology* **28**: 2541–2554.

Bernacchi CJ, Bagley JE, Serbin SP, Ruiz-Vera UM, Rosenthal DM, Vanloocke A. 2013. Modelling C3 photosynthesis from the chloroplast to the ecosystem. *Plant, Cell & Environment* **36**: 1641–1657.

Billman GE. 2020. Homeostasis: the underappreciated and far too often ignored central organizing principle of physiology. *Frontiers in Physiology* **11**: 200.

Blonder B, Escobar S, Kapás RE, Michaletz ST. 2020. Low predictability of energy balance traits and leaf temperature metrics in desert, montane and alpine plant communities. *Functional Ecology* **34**: 1882–1897.

Blonder B, Michaletz ST. 2018. A model for leaf temperature decoupling from air temperature. *Agricultural and Forest Meteorology* **262**: 354–360.

Campbell GS, Norman JM. 2012. *An introduction to environmental biophysics*. Berlin, Germany: Springer Science & Business Media.

Cavaleri MA. 2020. Cold-blooded forests in a warming world. *New Phytologist* **228**: 1455–1457.

Choury Z, Wujeska-Klause A, Bourne A, Bown NP, Tjoelker MG, Medlyn BE, Crous KY. 2022. Tropical rainforest species have larger increases in temperature optima with warming than warm-temperate rainforest trees. *New Phytologist* **234**: 1220–1236.

Collier CJ, Ow YX, Langlois L, Uthicke S, Johansson CL, O'Brien KR, Hrebien V, Adams MP. 2017. Optimum temperatures for net primary productivity of three tropical seagrass species. *Frontiers in Plant Science* **8**: 1446.

Dong N, Prentice IC, Harrison SP, Song QH, Zhang YP. 2017. Biophysical homoeostasis of leaf temperature: a neglected process for vegetation and land-surface modelling. *Global Ecology and Biogeography* **26**: 998–1007.

Doughty CE, Goulden ML. 2008. Are tropical forests near a high temperature threshold? *Journal of Geophysical Research: Biogeosciences* **113**: 1–12.

Drake JE, Harwood R, Vårhammar A, Barbour MM, Reich PB, Barton CV, Tjoelker MG. 2020. No evidence of homeostatic regulation of leaf temperature in *Eucalyptus parramattensis* trees: integration of CO_2 flux and oxygen isotope methodologies. *New Phytologist* **228**: 1511–1523.

Duman T, Huang CW, Litvak ME. 2021. Recent land cover changes in the Southwestern US lead to an increase in surface temperature. *Agricultural and Forest Meteorology* **297**: 108246.

Duveiller G, Hooker J, Cescatti A. 2018. The mark of vegetation change on Earth's surface energy balance. *Nature Communications* **9**: 1–12.

Ehleringer J, Björkman O, Mooney HA. 1976. Leaf pubescence: effects on absorptance and photosynthesis in a desert shrub. *Science* **192**: 376–377.

Ellsworth DS, Reich PB. 1993. Canopy structure and vertical patterns of photosynthesis and related leaf traits in a deciduous forest. *Oecologia* **96**: 169–178.

Fang H, Baret F, Plummer S, Schaepman-Strub G. 2019. An overview of global leaf area index (LAI): methods, products, validation, and applications. *Reviews of Geophysics* **57**: 739–799.

Farella MM, Fisher JB, Jiao W, Key KB, Barnes ML. 2022. Thermal remote sensing for plant ecology from leaf to globe. *Journal of Ecology* **110**: 1996–2014.

Farquhar GD, von Caemmerer SV, Berry JA. 1980. A biochemical model of photosynthetic CO_2 assimilation in leaves of C_3 species. *Planta* **149**: 78–90.

Fauset S, Freitas HC, Galbraith DR, Sullivan MJ, Aidar MP, Joly CA, Phillips OL, Vieira SA, Gloor MU. 2018. Differences in leaf thermoregulation and water use strategies between three co-occurring Atlantic forest tree species. *Plant, Cell & Environment* **41**: 1618–1631.

Forzieri G, Miralles DG, Ciais P, Alkama R, Ryu Y, Duveiller G, Zhang K, Robertson E, Kautz M, Martens B *et al.* 2020. Increased control of vegetation on global terrestrial energy fluxes. *Nature Climate Change* **10**: 356–362.

Friedl M, Sulla-Menashe D. 2019. *MCD12Q1 - MODIS/Terra+Aqua land cover type yearly L3 global 500m SIN grid V006*. Sioux Falls, SD, USA: NASA EOSDIS Land Processes DAAC [WWW document] URL https://lpdaac.usgs.gov/products/mcd12q1v006/.

García-Palacios P, Gross N, Gaitán J, Maestre FT. 2018. Climate mediates the biodiversity–ecosystem stability relationship globally. *Proceedings of the National Academy of Sciences, USA* **115**: 8400–8405.

Gates DM. 1965. Energy, plants, and ecology. *Ecology* **46**: 1–13.

Gibbons JD, Chakraborti S. 2014. *Nonparametric statistical inference*. Boca Raton, FL, USA: CRC Press.

Gray J, Sulla-Menashe D, Friedl MA. 2019. *User guide to collection 6 modis land cover dynamics (mcd12q2) product*. Missoula, MT, USA: NASA EOSDIS Land Processes DAAC [WWW document] URL https://modis-land.gsfc.nasa.gov/pdf/MODIS_Land_Cover_Dynamics_MCD12Q2_C61_Product.pdf.

Guo Z, Yan Z, Majcher BM, Lee CK, Zhao Y, Song G, Wang B, Wang X, Deng Y, Michaletz ST. 2022. Dynamic biotic controls of leaf thermoregulation across the diel timescale. *Agricultural and Forest Meteorology* **315**: 108827.

Huang M, Piao S, Ciais P, Peñuelas J, Wang X, Keenan TF, Peng S, Berry JA, Wang K, Mao J. 2019. Air temperature optima of vegetation productivity across global biomes. *Nature Ecology & Evolution* **3**: 772–779.

Hulley G, Freepartner R, Malakar N, Sarkar S. 2016. *Moderate Resolution Imaging Spectroradiometer (MODIS) Land Surface Temperature and Emissivity Product (MxD21) user guide*. Washington, DC, USA: NASA [WWW document] URL https://modis-land.gsfc.nasa.gov/pdf/MxD21_LST&E_UserGuide_C61.pdf.

Iio A, Hikosaka K, Anten NP, Nakagawa Y, Ito A. 2014. Global dependence of field-observed leaf area index in woody species on climate: a systematic review. *Global Ecology and Biogeography* **23**: 274–285.

Javadian M, Smith WK, Lee K, Knowles JF, Scott RL, Fisher JB, Moore DJ, van Leeuwen WJ, Barron-Gafford G. 2022. Canopy temperature is regulated by ecosystem structural traits and captures the ecohydrologic dynamics of a semiarid mixed conifer forest site. *Journal of Geophysical Research: Biogeosciences* **127**: e2021JG006617.

Jones HG. 2013. *Plants and microclimate: a quantitative approach to environmental plant physiology*. Cambridge, UK: Cambridge University Press.

Kattenborn T, Fassnacht FE, Schmidtlein S. 2019. Differentiating plant functional types using reflectance: which traits make the difference? *Remote Sensing in Ecology and Conservation* **5**: 5–19.

Kattge J, Diaz S, Lavorel S, Prentice IC, Leadley P, Bönisch G, Garnier E, Westoby M, Reich PB, Wright IJ. 2011. TRY – a global database of plant traits. *Global Change Biology* **17**: 2905–2935.

Leuzinger S, Körner C. 2007. Tree species diversity affects canopy leaf temperatures in a mature temperate forest. *Agricultural and Forest Meteorology* **146**: 29–37.

Lian X, Zeng Z, Yao Y, Peng S, Wang K, Piao S. 2017. Spatiotemporal variations in the difference between satellite-observed daily maximum land surface temperature and station-based daily maximum near-surface air temperature. *Journal of Geophysical Research: Atmospheres* **122**: 2254–2268.

Lin H, Tu C, Fang J, Gioli B, Loubet B, Gruening C, Zhou G, Beringer J, Huang J, Dušek J *et al.* 2020. Forests buffer thermal fluctuation better than non-forests. *Agricultural and Forest Meteorology* **288**: 107994.

Linacre ET. 1964. A note on a feature of leaf and air temperatures. *Agricultural Meteorology* **1**: 66–72.

Lloyd J, Farquhar GD. 2008. Effects of rising temperatures and [CO_2] on the physiology of tropical forest trees. *Philosophical Transactions of the Royal Society of London. Series B: Biological Sciences* **363**: 1811–1817.

Lombardozzi DL, Bonan GB, Smith NG, Dukes JS, Fisher RA. 2015. Temperature acclimation of photosynthesis and respiration: a key uncertainty in the carbon cycle-climate feedback. *Geophysical Research Letters* **42**: 8624–8631.

Mahan JR, Upchurch DR. 1988. Maintenance of constant leaf temperature by plants—I. Hypothesis-limited homeothermy. *Environmental and Experimental Botany* **28**: 351–357.

Medina S, Vicente R, Nieto-Taladriz MT, Aparicio N, Chairi F, Vergara-Diaz O, Araus JL. 2019. The plant-transpiration response to vapor pressure deficit (VPD) in durum wheat is associated with differential yield performance and specific expression of genes involved in primary metabolism and water transport. *Frontiers in Plant Science* **9**: 1994.

Michaletz ST, Weiser MD, McDowell NG, Zhou J, Kaspari M, Helliker BR, Enquist BJ. 2016. The energetic and carbon economic origins of leaf thermoregulation. *Nature Plants* **2**: 1–9.

Muñoz-Sabater J, Dutra E, Agustí-Panareda A, Albergel C, Arduini G, Balsamo G, Boussetta S, Choulga M, Harrigan S, Hersbach H. 2021. ERA5-land: a state-of-the-art global reanalysis dataset for land applications. *Earth System Science Data* **13**: 4349–4383.

Myneni R, Knyazikhin Y, Park T. 2015. *MCD15A3H MODIS/Terra+ aqua leaf area index/FPAR 4-day L4 global 500 m SIN Grid V006 [data set]*. Missoula, MT, USA: NASA EOSDIS Land Processes DAAC.

Novick KA, Ficklin DL, Stoy PC, Williams CA, Bohrer G, Oishi AC, Papuga SA, Blanken PD, Noormets A, Sulman BN. 2016. The increasing importance of atmospheric demand for ecosystem water and carbon fluxes. *Nature Climate Change* **6**: 1023–1027.

Parker WS. 2016. Reanalyses and observations: what's the difference? *Bulletin of the American Meteorological Society* **97**: 1565–1572.

Pastorello G, Trotta C, Canfora E, Chu H, Christianson D, Cheah YW, Poindexter C, Chen J, Elbashandy A, Humphrey M *et al.* 2020. The FLUXNET2015 dataset and the ONEFlux processing pipeline for eddy covariance data. *Scientific Data* **7**: 225.

Pau S, Detto M, Kim Y, Still CJ. 2018. Tropical forest temperature thresholds for gross primary productivity. *Ecosphere* **9**: e02311.

Pekel JF, Cottam A, Gorelick N, Belward AS. 2016. High-resolution mapping of global surface water and its long-term changes. *Nature* **540**: 418–422.

Peng SS, Piao S, Zeng Z, Ciais P, Zhou L, Li LZ, Myneni RB, Yin Y, Zeng H. 2014. Afforestation in China cools local land surface temperature. *Proceedings of the National Academy of Sciences, USA* **111**: 2915–2919.

Perera RS, Cullen BR, Eckard RJ. 2019. Using leaf temperature to improve simulation of heat and drought stresses in a biophysical model. *Plants* **9**: 8.

Poulter B, MacBean N, Hartley A, Khlystova I, Arino O, Betts R, Bontemps S, Boettcher M, Brockmann C, Defourny P. 2015. Plant functional type classification for earth system models: results from the European Space Agency's Land Cover Climate Change Initiative. *Geoscientific Model Development* **8**: 2315–2328.

Ryu Y, Baldocchi DD, Kobayashi H, Van Ingen C, Li J, Black TA, Beringer J, Van Gorsel E, Knohl A, Law BE. 2011. Integration of MODIS land and atmosphere products with a coupled-process model to estimate gross primary productivity and evapotranspiration from 1 km to global scales. *Global Biogeochemical Cycles* **25**: 4.

Sadok W, Jagadish SK. 2020. The hidden costs of nighttime warming on yields. *Trends in Plant Science* **25**: 644–651.

Slot M, Winter K. 2017. In situ temperature response of photosynthesis of 42 tree and liana species in the canopy of two Panamanian lowland tropical forests with contrasting rainfall regimes. *New Phytologist* **214**: 1103–1117.

Smith WK, Carter GA. 1988. Shoot structural effects on needle temperatures and photosynthesis in conifers. *American Journal of Botany* **75**: 496–500.

Still C, Powell R, Aubrecht D, Kim Y, Helliker B, Roberts D, Richardson AD, Goulden M. 2019. Thermal imaging in plant and ecosystem ecology: applications and challenges. *Ecosphere* **10**: e02768.

Still CJ, Page G, Rastogi B, Griffith DM, Aubrecht DM, Kim Y, Burns SP, Hanson CV, Kwon H, Hawkins L *et al.* 2022. No evidence of canopy-scale leaf thermoregulation to cool leaves below air temperature across a range of forest ecosystems. *Proceedings of the National Academy of Sciences, USA* **119**: e2205682119.

Still CJ, Rastogi B, Page GF, Griffith DM, Sibley A, Schulze M, Hawkins L, Pau S, Detto M, Helliker BR. 2021. Imaging canopy temperature: shedding (thermal) light on ecosystem processes. *New Phytologist* **230**: 1746–1753.

Thakur S, Maity D, Mondal I, Basumatary G, Ghosh PB, Das P, De TK. 2021. Assessment of changes in land use, land cover, and land surface temperature in the mangrove forest of Sundarbans, northeast coast of India. *Environment, Development and Sustainability* **23**: 1917–1943.

Wan Z. 2014. New refinements and validation of the collection-6 MODIS land-surface temperature/emissivity product. *Remote Sensing of Environment* **140**: 36–45.

Wang L, Lu Y, Yao Y. 2019. Comparison of three algorithms for the retrieval of land surface temperature from Landsat 8 images. *Sensors* **19**: 5049.

Wright IJ, Dong N, Maire V, Prentice IC, Westoby M, Díaz S, Gallagher RV, Jacobs BF, Kooyman R, Law EA. 2017. Global climatic drivers of leaf size. *Science* **357**: 917–921.

Wu J, Rogers A, Albert LP, Ely K, Prohaska N, Wolfe BT, Oliveira RC Jr, Saleska SR, Serbin SP. 2019. Leaf reflectance spectroscopy captures variation in carboxylation capacity across species, canopy environment and leaf age in lowland moist tropical forests. *New Phytologist* **224**: 663–674.

Wu S, Wang J, Yan Z, Song G, Chen Y, Ma Q, Deng M, Wu Y, Zhao Y, Guo Z. 2021. Monitoring tree-crown scale autumn leaf phenology in a temperate forest with an integration of PlanetScope and drone remote sensing observations. *ISPRS Journal of Photogrammetry and Remote Sensing* **171**: 36–48.

Yan Z, Guo Z, Serbin SP, Song G, Zhao Y, Chen Y, Wu S, Wang J, Wang X, Li J. 2021. Spectroscopy outperforms leaf trait relationships for predicting photosynthetic capacity across different forest types. *New Phytologist* **232**: 134–147.

Yang D, Morrison BD, Hantson W, Breen AL, McMahon A, Li Q, Salmon VG, Hayes DJ, Serbin SP. 2021. Landscape-scale characterization of Arctic tundra vegetation composition, structure, and function with a multi-sensor unoccupied aerial system. *Environmental Research Letters* **16**: 85005.

Zanaga D, Van De Kerchove R, De Keersmaecker W, Souverijns N, Brockmann C, Quast R, Wevers J, Grosu A, Paccini A, Vergnaud S *et al.* 2021. ESA WorldCover 10 m 2020 v100. *Zenodo.* doi: 10.5281/zenodo.5571936.

Zeng Z, Piao S, Li LZ, Zhou L, Ciais P, Wang T, Li Y, Lian XU, Wood EF, Friedlingstein P. 2017. Climate mitigation from vegetation biophysical feedbacks during the past three decades. *Nature Climate Change* **7**: 432–436.

Zeng Z, Wang D, Yang L, Wu J, Ziegler AD, Liu M, Ciais P, Searchinger TD, Yang ZL, Chen D. 2021. Deforestation-induced warming over tropical mountain regions regulated by elevation. *Nature Geoscience* **14**: 23–29.

Zhou D, Xiao J, Frolking S, Liu S, Zhang L, Cui Y, Zhou G. 2021. Croplands intensify regional and global warming according to satellite observations. *Remote Sensing of Environment* **264**: 112585.

Zhu Z, Piao S, Myneni RB, Huang M, Zeng Z, Canadell JG, Ciais P, Sitch S, Friedlingstein P, Arneth A. 2016. Greening of the Earth and its drivers. *Nature Climate Change* **6**: 791–795.

Zuur AF, Ieno EN, Walker NJ, Saveliev AA, Smith GM. 2009. *Mixed effects models and extensions in ecology with R, vol. 574.* New York, NY, USA: Springer.

Supporting Information

Additional Supporting Information may be found online in the Supporting Information section at the end of the article.

Fig. S1 Conceptual diagram of the plant thermoregulation (cf. fig. 1 of Drake *et al.*, 2020).

Fig. S2 Comparison between eddy covariance (EC)- and satellite-derived canopy temperature (T_c).

Fig. S3 Percentage data availability of Moderate Resolution Imaging Spectroradiometer (MODIS) land surface temperature (LST) satellite data (MYD11A2) on a global scale.

Fig. S4 Relationship between two indicators (slope and ΔT) of the canopy temperature (T_c) vs air temperature (T_a) relationship across 22 tropical flux sites.

Fig. S5 Workflow for studying the spatial and temporal variability of plant thermoregulation and its drivers on a global scale.

Fig. S6 Original and partial relationships between canopy-to-air temperature difference (ΔT) and leaf area index (LAI).

Fig. S7 Sensitivity analysis to evaluate the influence of different leaf area index (LAI) thresholds on the assessments of satellite-based canopy temperature (T_c) vs air temperature (T_a) relationships.

Fig. S8 Cross-comparison between aerodynamic canopy temperature (T_{c_aero}) and longwave canopy temperature (T_{c_LW}) across 94 eddy covariance (EC) sites.

Fig. S9 Mean passing times for Moderate Resolution Imaging Spectroradiometer (MODIS) Terra and Aqua satellite.

Fig. S10 Examples of temporal ΔT, LAI, PAR, RH, rainfall, and wind speed across the growing season in the AU-Wac forest site. ΔT, canopy-to-air temperature difference; LAI, leaf area index; PAR, photosynthetically active radiation; RH, relative humidity.

Fig. S11 Correlations among different explanatory variables.

Fig. S12 The residual patterns for the generalized linear model results (i.e. modeled T_c – observed T_c) based on eddy covariance (EC) data. T_c, canopy temperature.

Fig. S13 The residual patterns for the generalized linear model results (i.e. modeled T_c–observed T_c) based on satellite data. T_c, canopy temperature.

Fig. S14 Relative importance of the eight selected abiotic and biotic factors for explaining the global variability in the slope indicator of canopy temperature (T_c) vs air temperature (T_a) regression.

Fig. S15 Relationship between evapotranspiration (ET), canopy-to-air temperature difference (ΔT), and leaf area index (LAI).

Methods S1 Introduction of FLUXNET 2015, satellite, and ERA5-Land (ERA5L) reanalysis data.

Methods S2 Removing the evapotranspiration (ET) effect from canopy-to-air temperature difference (ΔT) vs leaf area index (LAI) relationship.

Table S1 Cross-comparing different versions of generalized linear models of plant thermoregulation capacities (canopy-to-air temperature difference, ΔT) based on the Akaike information criterion (AIC) metric.

Table S2 Relative importance of each driver for explaining the global variability in canopy-to-air temperature difference (ΔT) based on the best generalized linear model (that was selected based on the smallest Akaike information criterion (AIC) values shown in Table S1).

Please note: Wiley is not responsible for the content or functionality of any Supporting Information supplied by the authors. Any queries (other than missing material) should be directed to the *New Phytologist* Central Office.